Experimental application of FRF-based model updating approach to estimate soil mass and stiffness mobilised under pile impact tests

Prendergast, L. J.; Wu, W. H.; Gavin, K.

DOI
10.1016/j.soildyn.2019.04.027

Publication date
2019

Document Version
Final published version

Published in
Soil Dynamics and Earthquake Engineering

Soil Dynamics and Earthquake Engineering 123 (2019) 1–15

Contents lists available at ScienceDirect

Soil Dynamics and Earthquake Engineering

journal homepage: www.elsevier.com/locate/soildyn

Experimental application of FRF-based model updating approach to estimate soil mass and stiffness mobilised under pile impact tests

L.J. Prendergast[a,*], W.H. Wu[b], K. Gavin[c]

[a] Department of Civil Engineering, Faculty of Engineering, University of Nottingham, Nottingham, NG7 2RD, United Kingdom
[b] Department of Construction Engineering, National Yunlin University of Science and Technology, Section 3, Daxue Road, Douliu City, Yunlin 640, Taiwan
[c] Faculty of Civil Engineering and Geosciences, Delft University of Technology, Building 23, Stevinweg 1 / PO-box 5048, 2628 CN Delft, 2600 GA, Delft, the Netherlands

ARTICLE INFO

Keywords:
Soil stiffness
Model-updating
Dynamics
Mass
Winkler
Soil-structure interaction

ABSTRACT

The dynamic response of structures in contact with soil is receiving increasing interest and there is a growing need for more accurate models capable of simulating the behaviour of these systems. This is particularly important in the field of offshore wind turbines, where accurate estimates of system frequency are needed to avoid resonance, and in the structural health monitoring fields, where accurate reference damage models are used. Previous work has shown that there is significant uncertainty in how to specify mobilised soil stiffness for dynamic soil-pile interaction modelling. Moreover, the contribution of soil mass in dynamic motion is often ignored. This paper applies a finite-element iterative model updating approach previously developed by the authors to two experimental piles to ascertain the mobilised soil stiffness and mass profiles from impact test data. The method works by obtaining a frequency response function (FRF) from an impact test performed on a test pile, developing a numerical model of this system, applying initial estimates of soil mass and stiffness, and updating these properties to match the experimental FRF with that generated in the numerical model. A range of elements are investigated including multiple runs of the approach to test repeatability, the influence of different starting estimates for stiffness, the effect of variability in experimental test data, and the influence of the pile length over which masses are distributed. Moreover, potential sources of error are discussed. The method provides reasonably consistent estimates of the soil stiffness and mass acting in the lateral dynamic motion of a given pile tested in this paper. The approach may be useful in the continued improvement of Soil-Structure Interaction (SSI) modelling for dynamic applications.

1. Introduction

There is increasing interest in the dynamic response of structures incorporating soil-structure interaction, particularly in the fields of Earthquake [1,2] and Offshore Engineering [3–6] among others. For offshore wind turbines, accurate knowledge of the soil-structure interaction behaviour is paramount to the safe operation of these structures due to the potential for resonance from waves and the spinning rotor, which can exacerbate fatigue. In recent times, the field of vibration-based Structural Health Monitoring (SHM), which traditionally focussed on detecting damage in super-structural components such as bridge beams [7–9], has begun to focus on damage detection of foundations [10–14]. These recent developments have led to an urgency relating to the need for accurate models capable of encapsulating the behaviour of soil-structure interaction systems.

The development of numerical models for structural simulations has been the recourse for design engineers for many years, since it is not possible to experimentally trial every load-case a structure may incur. It is unusual for a developed numerical model of a given structural system to perfectly model the behaviour at the first trial, therefore the field of Finite-Element (FE) model updating has focussed on utilising information from the actual structural response to modify the parameters of the numerical model in order to minimise the differences in behaviour between the model and the real system. This is particularly important in the field of structural damage detection where reference numerical models of assets such as bridges are required to benchmark normal operating behaviour. In dynamic modelling fields, model updating approaches have received much attention in recent years [15–23]. Imregun et al. [15] developed a Frequency Response Function (FRF)-based model updating approach and investigated its performance against several barriers for implementation including noisy experimental data and the uniqueness of the updated model when applied to the case of a

* Corresponding author.
E-mail addresses: luke.prendergast@nottingham.ac.uk (L.J. Prendergast), wuwh@yuntech.edu.tw (W.H. Wu), k.g.gavin@tudelft.nl (K. Gavin).

https://doi.org/10.1016/j.soildyn.2019.04.027
Received 18 September 2018; Received in revised form 23 February 2019; Accepted 24 April 2019

beam. Experimental noise posed an issue to the accuracy of the method. Nalitolela et al. [16] demonstrated a FRF-based approach using experimental and simulated data, which was based on the addition of artificial stiffness to the structure. A sensitivity procedure was used to update the model parameters. Esfandiari et al. [20] developed a model updating approach to identify the presence of damage by updating the stiffness and mass of the structure using a FRF-based method applied to a truss model. A similar study by Hwang and Kim [18] focussed on estimating damage severity and location using FRFs for a cantilever beam and a helicopter rotor blade model. Wu et al. [23] presented a FRF-based approach to estimate the mass and stiffness of soil contributing to the lateral dynamic motion of simulated foundation piles, and demonstrated the method using numerically simulated data for typical pile geometries and soil spring stiffness.

This paper is an advancement on work presented by Prendergast and Gavin [6] and Wu et al. [23]. Prendergast and Gavin [6] investigated the variation in modelled dynamic response of soil-pile systems through the implementation of different formulations of soil spring stiffness. The various formulations, termed coefficients of subgrade reaction (in static case), require the specification of pile structural and geometric parameters such as Young's modulus (E), second moment of area (I), pile diameter (D) and soil properties including small-strain stiffness (E_0) and Poisson's ratio (v_s). These expressions, originally derived for static applications under specified operational strain, led to significantly varied dynamic responses in the study conducted in Ref. [6], both in predicted acceleration magnitude and frequency. This study highlighted the significant uncertainty that persists in the selection of an appropriate subgrade reaction model to transform identical soil and pile properties, as significantly different responses were predicted. The present study applies the FRF-based model updating approach developed by Wu et al. [23] to the experimental case study data of two piles in Ref. [6], with a view to estimating the soil mass and stiffness mobilised in the dynamic motion. The FRF of a given pile is derived using the input force time-history and the output acceleration-time history from experimental testing, and this is used as the target in the updating method. A numerical beam-Winkler model is developed with an initial soil stiffness profile, estimated using a variety of subgrade reaction formulations and available geotechnical data [6]. This stiffness is applied in the numerical model and the soil mass is initially guessed. The method then updates the stiffness and mass at the soil-structure interface in the beam-Winkler model until the experimental FRF and the numerical FRF generated in the model match within a defined tolerance. The approach aims to reduce the uncertainty in the selection of a soil stiffness profile by enabling a simple model updating approach using a single FRF from the target structure.

2. Numerical modelling of piles

In this section, the methods adopted to formulate numerical FE models of piles to model their dynamic responses are described.

2.1. Mathematical formulation

Numerical beam-Winkler models are developed to simulate the behaviour of real test piles, described in Section 4. A FE model from which to obtain the dynamic response of a pile to a lateral impact is modelled in this paper using Euler-Bernoulli beam elements [24] to model the pile, and Winkler spring elements [25,26] to model the soil. Soil mass is incorporated by adding lumped masses to the nodes connecting Winkler spring elements to the pile elements. The global dynamic response is governed by Eq. (1).

$$M_G\{\ddot{X}(t)\} + C_G\{\dot{X}(t)\} + K_G\{X(t)\} = \{P(t)\} \tag{1a}$$

where $\mathbf{M_G}$, $\mathbf{C_G}$ and $\mathbf{K_G}$ are the $(N \times N)$ global mass, damping and stiffness matrices for the pile-soil system; N is the total number of degrees of freedom (DOF) and

$$X(t) = \{x_1(t) \quad x_2(t).....x_N(t)\}^T \tag{1b}$$

$$\dot{X}(t) = \{\dot{x}_1(t) \quad \dot{x}_2(t).....\dot{x}_N(t)\}^T \tag{1c}$$

$$\ddot{X}(t) = \{\ddot{x}_1(t) \quad \ddot{x}_2(t).....\ddot{x}_N(t)\}^T \tag{1d}$$

$$P(t) = \{p_1(t) \quad p_2(t).....p_N(t)\}^T \tag{1e}$$

where $X(t)$, $\dot{X}(t)$ and $\ddot{X}(t)$ are the displacement, velocity and acceleration of each DOF in the model, for each time step. Damping is modelled using Cauchy damping, employing a two-term Rayleigh formulation [27]. The damping ratio used is measured from the experimental signals, see Section 4. The dynamic response is obtained by solving Eq. (1) using the Wilson-θ integration scheme [28,29]. The natural frequencies and mode shapes of the soil-pile system may be calculated by solving the Eigenproblem [27] of the system matrix $\mathbf{D_{SYS}} = \mathbf{M_G}^{-1}\mathbf{K_G}$. Further details on the numerical modelling employed are available in Wu et al. [23]. In this paper, the mass and stiffness matrices for the pile model are derived using the material and geometrical properties of the test piles, described in Section 4. The force vector $P(t)$ is populated using the force time-history from a modal hammer impact, described in Section 4.

2.2. Soil stiffness using subgrade reaction approach

The present paper is an evolution of work presented by Prendergast and Gavin [6] which assessed the performance of five particular formulations of subgrade reaction in modelling the small-strain dynamic response of laterally vibrating piles. These models were developed by Biot [30], see Eq. (2), Vesic [31,32], see Eq. (3), Meyerhof and Baike [33,34], see Eq. (4), Klopple and Glock [33–35], see Eq. (5) and Selvadurai [34,35], see Eq. (6). The research in Ref. [6] concluded that for the given field conditions and pile parameters considered, the Vesic model (Eq. (3)) provided the closest approximation to the frequency response of two experimental piles, with deviations of 16.6% and 3.9% respectively. However, the analysis highlighted the significant disparity in predicted response depending on which formulation was implemented, and moreover the analysis assumed no soil mass contributed to the dynamic behaviour of the pile-soil system. In this paper, these subgrade reaction models are used to specify the initial stiffness guess in the model-updating approach.

$$k_s = \frac{0.95E_0}{D(1-v_s^2)}\left[\frac{E_0D^4}{(1-v_s^2)EI}\right]^{0.108} \tag{2}$$

$$k_s = \frac{0.65E_0}{D(1-v_s^2)}\left[\frac{E_0D^4}{EI}\right]^{1/12} \tag{3}$$

$$k_s = \frac{E_0}{D(1-v_s^2)} \tag{4}$$

$$k_s = \frac{2E_0}{D(1+v_s)} \tag{5}$$

$$k_s = \frac{0.65}{D}\frac{E_0}{(1-v_s^2)} \tag{6}$$

where E_0 is the small-strain Young's modulus of soil (N/m^2), D is the pile diameter (m), v_s is the Poisson ratio, E is the Young's modulus of the pile material (N/m^2) and I is the cross-sectional moment of inertia (m^4). The E_0 profile for a given site can be estimated using shear wave velocity measurements [36,37], or from correlations to other geotechnical site investigation tests such as Cone Penetration Test (CPT) data [3,38–40]. The method for converting the moduli of subgrade reaction to individual spring moduli is detailed in Prendergast et al. [13].

3. Soil mass and stiffness iterative updating method

A graphical representation of the model updating approach

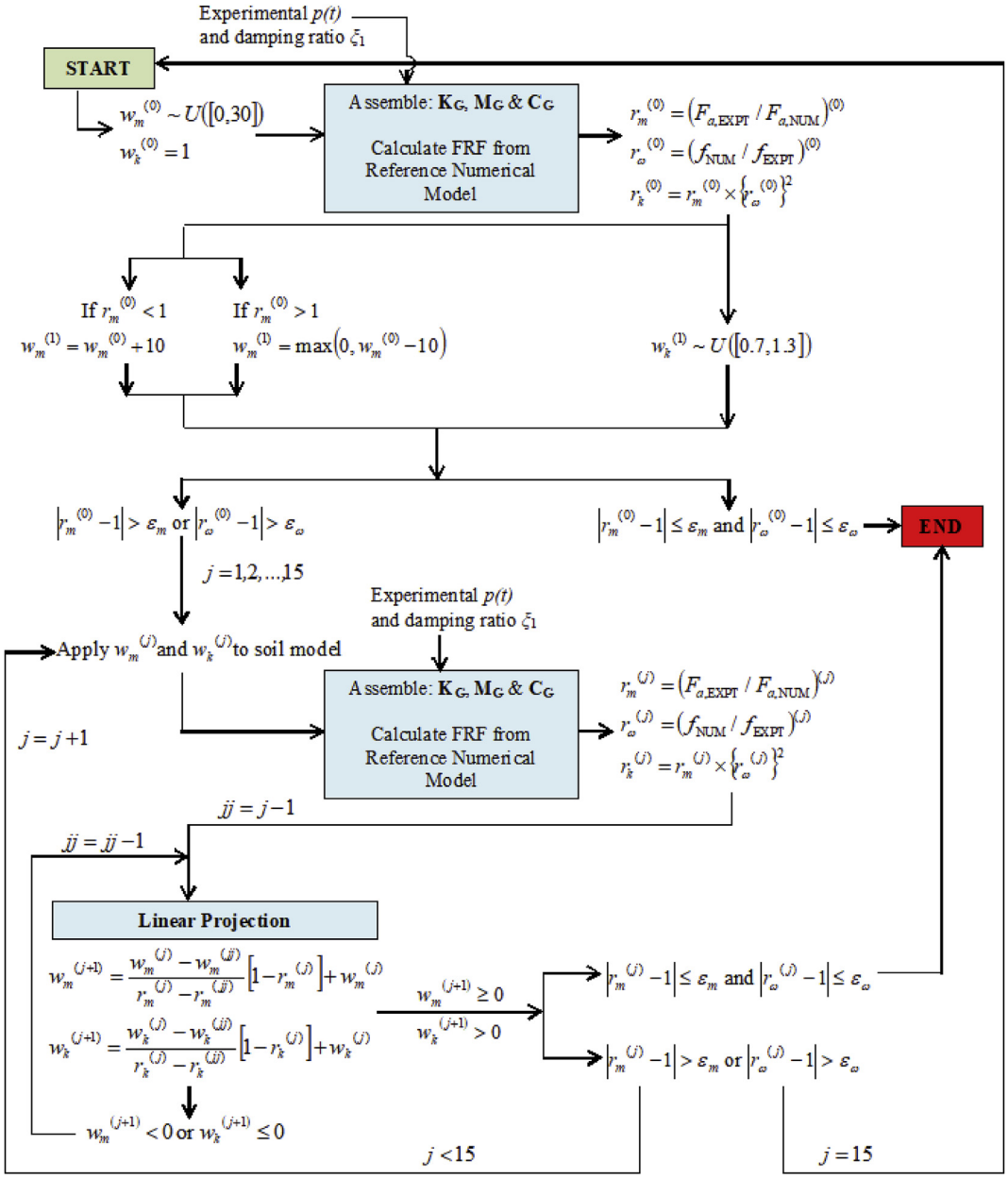

Fig. 1. Flow chart of iterative algorithm.

developed by Wu et al. [23] to estimate the soil mass and stiffness acting along a pile is shown in Fig. 1 and an overview of the procedure is summarised herein.

An experimental FRF is obtained from an impact test on the pile for which the soil stiffness and mass are sought, using Eq. (7) [6,41,42].

$$H_a(\bar{\omega}) = \frac{\ddot{X}(\bar{\omega})}{F(\bar{\omega})} \tag{7}$$

where $P(\bar{\omega})$ is the Fourier transform of the input force time-history $p(t)$ from a modal hammer and $\ddot{X}(\bar{\omega})$ is the Fourier transform of the output acceleration time-history $\ddot{x}(t)$ from an accelerometer. The amplitude of the complex-valued FRF in Eq. (7) is denoted by $F_a(\bar{\omega}) = |H_a(\bar{\omega})|$. It is assumed that the material and geometry of this pile are known to the user so that a *reference* beam-Winkler numerical model of the system can be created using the approach in Section 2.1. Using site investigation data such as shear wave measurements and employing a subgrade reaction model such as in Eqs. (2)–(6), soil spring stiffnesses can be applied in the numerical model as the initial *educated guess* as to the acting soil stiffness in the system. A stiffness weighting, w_k is initially assumed as 1 times this profile. An initial guess of soil mass is postulated from a uniform distribution of mass weightings, w_m between 0 and 30, to be multiplied by the known pile mass, m_p and distributed among the sprung pile nodes in the reference numerical model. The information is used to assemble mass, $\mathbf{M_G}$ and stiffness, $\mathbf{K_G}$ matrices using the approach in Section 2.1. The numerical model also requires an estimate of the damping of the real system and, as a Rayleigh formulation is adopted in the modelling, the damping ratio of the first mode ξ_1 is required. This can be estimated from the experimental time-domain response using the logarithmic decrement technique [43] or through fitting exponential decay functions [44]. This can also be estimated in the frequency domain using the half-power bandwidth method [43]. The damping matrix $\mathbf{C_G}$ is then formulated as a linear combination of $\mathbf{M_G}$ and $\mathbf{K_G}$, using this specified damping ratio [27]. Once a numerical model employing an initial guess of the soil properties of the real system is developed, one can generate a first estimate numerical FRF by applying the force time-history from the experimental test to a node in

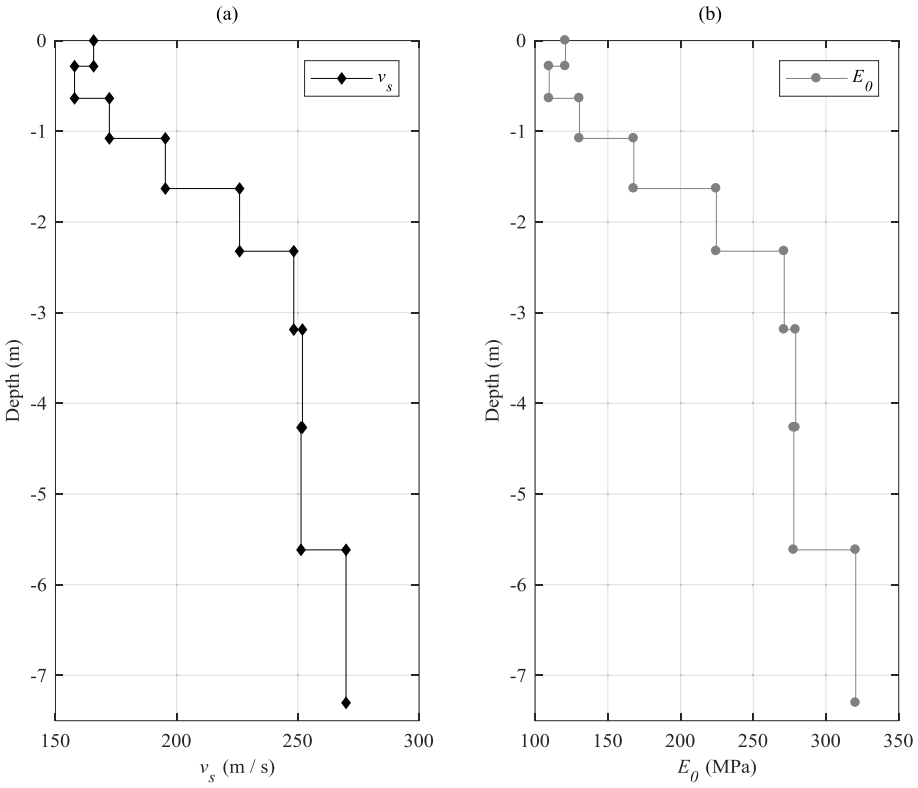

Fig. 2. Small-strain soil stiffness data. (a) Shear wave velocity measurements, (b) derived E_0 profile.

the numerical model close to the point of application on the real system, and the acceleration response of the system may be calculated by solving Eq. (1). The output acceleration from the node closest to the accelerometer on the real system is used in the FRF specification. After the first run of the numerical model, one now has a FRF from the experimental test, and a FRF from the numerical model. A mass ratio is defined as $r_m = F_{a,EXPT}/F_{a,NUM}$ where $F_{a,EXPT}$ is the peak amplitude of the experimental acceleration FRF and $F_{a,NUM}$ is the peak amplitude of the calculated numerical FRF. A frequency ratio is defined as $r_\omega = f_{NUM}/f_{EXPT}$ where f_{NUM} is the frequency associated with $F_{a,NUM}$ and f_{EXPT} is the frequency associated with $F_{a,EXPT}$. The peak information (amplitude and frequency) from both FRFs can be used to obtain r_m, r_ω and subsequently to calculate $r_k = r_m \times (r_\omega)^2$. These values are stored for use later in the linear projection. Two convergence criteria are defined; ε_ω is the frequency convergence tolerance and ε_m is mass convergence tolerance. For all experimental trials in this paper, the convergence criteria are set to 1%.

For the second run of the iterative method, the soil mass estimate is either increased or decreased depending on the magnitude of r_m from the initial run. If $r_m^{(0)} < 1$, the mass should increase as this was underestimated in the numerical model in the first run. If $r_m^{(0)} > 1$, the mass weighting should decrease. The mass weighting is increased or decreased by an arbitrary value of 10 for the second guess, with a minimum mass of zero applied (no negative mass). The value '10' is not important, as the actual mass weighting is calculated in later iterations using the two starting estimates from iteration$^{(0)}$ and iteration$^{(1)}$. For the stiffness weighting, the second guess is chosen from a uniform distribution of values between 0.7 and 1.3, to be multiplied by the initial soil stiffness profile. Once again, the actual value is unimportant, as two starting estimates are required in the iterative approach to allow the system minimise the difference in the FRF peak information and converge on mobilised weightings to be applied to the stiffness and mass estimates. Once the second run stiffness and mass weightings are specified (and stored), the system checks if the results of the initial first run are within the defined tolerance, i.e. less than 1% difference in FRF peak amplitudes and frequencies between experimental and numerical FRFs. If they are not, the second guess weightings are applied to the profiles in the numerical model. New $\mathbf{M_G}$, $\mathbf{K_G}$ and $\mathbf{C_G}$ matrices are assembled, the force time-history is applied, the output acceleration is calculated, and a new FRF is generated. There now exists two estimates of the FRF of the system, iteration$^{(0)}$ and iteration$^{(1)}$. Both of these estimates are used to initiate the linear projection method to calculate further weightings for stiffness and mass towards convergence. These further weightings are updated using the mass ratio, r_m, and the frequency ratio, r_ω, from the current and previous iterations, and the stiffness ratio defined by $r_k = r_m \times (r_\omega)^2$. The linear projection aims to minimise the difference in FRF peak value and frequency between the generated numerical FRF and the target experimental FRF. Once the calculated weightings lead to the generation of a numerical FRF that converges on the experimental FRF, the method terminates and outputs the converged soil stiffness profile and added soil mass.

Due to the tendency for error propagation in automated optimisation processes, some inadmissibility checks and boundary conditions are implemented in the procedure. It is possible for the linear projection method to postulate a negative weighting for stiffness or mass. If this happens, the linear projection method automatically re-calculates the new weighting using the *j*th and *(j-2)*th, *j*th and *(j-3)*th … *j*th and *(j-i)*th iterations until admissible weightings are produced. Should the *(j-i)*th iteration reach the first iteration of the method without an admissible weighting being obtained, the new weighting is calculated by multiplying the value of the *j*th iteration by a random value between 0.9 and 1.1 (i.e. the current weighting is varied by ± 10%), then the method continues as normal. Additionally, if convergence is not achieved within (an arbitrary) 15 iterations, the system resets and re-initialises all of the parameters.

4. Experimental pile tests

Data from a field test conducted in Prendergast and Gavin [6] is used to test the iterative updating approach developed in Wu et al. [23].

A summary of the field test and information relating to the new analysis is described herein. Lateral vibration tests were conducted on two 0.34 m diameter open-ended steel piles driven into dense, over-consolidated sand at a quarry in Blessington, southwest of Dublin, Ireland. Prior to testing, both piles were excavated by different amounts to give L/D ratios of 13 and 9 for Pile 1 and 2, respectively, see Fig. 6(a).

The test quarry has been characterised in detail [45] and used to investigate the performance of a number of model, prototype and full scale foundation concepts over the last number of years [46–49]. A full description of the geotechnical properties of the site can be obtained in Refs. [37,45,46,50]. The small-strain stiffness properties of the site, measured using Multi-Channel Analysis of Surface Waves (MASW), see Ref. [36], are required for the approach in this paper. The shear wave velocity profile, Fig. 2(a) is used to derive the small-strain Young's modulus profile, Fig. 2(b) by first calculating the small-strain shear modulus (G_0) using $G_0 = \rho v_s^2$ and $E_0 = 2G_0(1 + \nu)$, where ρ is the soil density (kg/m^3) and ν is the small-strain Poisson ratio, taken as 0.1.

Each pile was fitted with three accelerometers distributed along the exposed portion of the pile shaft, see Fig. 6(a), and these accelerometers were programmed to scan at 1000 Hz. Note, only the top accelerometer is used in the procedure while the remaining two accelerometers are used to ensure consistency in the data. The test procedure (for a given pile) involved impacting the pile laterally with a PCB Piezotronics 086D50 model sledgehammer-type modal hammer [51](tip mass = 5.5 kg) and measuring the resulting acceleration signal from the accelerometers, see Fig. 3. A number of hammer impacts were undertaken on each pile to investigate repeatability. Each acceleration signal was low-pass filtered with a cut-off at 60 Hz to reduce the contribution of higher modes and noise, and a FRF is then generated, which is used as the target data in the numerical analysis to estimate the stiffness and mass contribution of the soil.

The damping ratio is estimated for each impact test by fitting an exponential curve to the peaks of the filtered acceleration signal in the time-domain, see Refs. [6,44], and validated using a logarithmic decrement technique [43].

FRFs of velocity and displacement are derived from the acceleration FRF using Eqs. (8) and (9). These FRFs are used to test the convergence of the iterative approach in the sense that if the converged soil mass and stiffness estimates provide a match in F_a, F_v and F_d, this acts as an additional check to mitigate false positives. Note, F_v and F_d are not used directly in the iterative updating approach (see Fig. 1), but only used as a check in the converged model. Note also that these are derived from F_a because the pile velocity and displacement are not measured in the experiment.

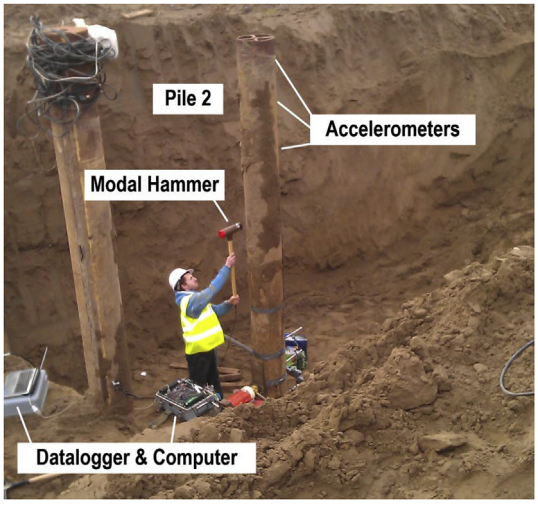

Fig. 3. Photo of impact testing on Pile 2.

$$F_v(\bar{\omega}) = \left|\frac{H_a(\bar{\omega})}{i\bar{\omega}}\right| = \frac{F_a(\bar{\omega})}{\bar{\omega}} \tag{8}$$

$$F_d(\bar{\omega}) = \left|\frac{H_a(\bar{\omega})}{(i\bar{\omega})^2}\right| = \frac{F_a(\bar{\omega})}{\bar{\omega}^2} \tag{9}$$

where $\bar{\omega}$ is the variable of excitation. The FRFs for five impact tests conducted on Pile 1 and 2 respectively are shown in Fig. 4 and the data is presented in Table 1. Damping data specified is from the curve fitting approach. Fig. 4(a) shows the frequency content of the force time-histories for the five impacts applied to Pile 1. Fig. 4(b) shows the acceleration FRFs for these five impacts on Pile 1. Fig. 4(c) shows the frequency content of the force time-histories for the five impacts applied to Pile 2. Fig. 4(d) shows the acceleration FRFs for these five impacts on Pile 2. The frequency content of the force-time histories is relatively uniform in the range of interest in this paper.

Using Eqs. (8) and (9), F_a can be converted to F_v and F_d. Fig. 5 shows the derived F_v and F_d from the first impact test conducted on both Pile 1 and Pile 2. These are used as a means to check the converged mass and stiffness weightings at the end of applying the method.

5. Analysis

5.1. Numerical modelling of field data

Two field piles were experimentally tested, as described in Section 4. Two reference numerical models were developed, shown in Fig. 6(b) and (c) for Pile 1 and 2 respectively, using the procedure described in Section 2.1. Pile 1 contains 72 Euler-Bernoulli beam elements, each of length 0.1 m, and 46 Winkler spring elements to model the soil. Since Pile 1 was initially excavated from an embedment of 7 m–4.5 m, there still exists soil within the pile (as it is an open-ended tube). The level of internal soil (plug) was approximately 2 m below the original ground level. This was incorporated in the numerical model as an extra mass, assuming a (packed) density for the internal soil at 2000 kg/m^3. External soil (added) masses are initially set to zero except for the top quarter of the springs, in line with the procedure in Ref. [23], due to the fact that an embedded pile impacted laterally at the head will have little modal displacement at depth (Section 5.6 investigates apportioning masses over increasing portions of the piles). The external impact force is applied at a distance of 1 m below the pile head, close to the point of application on the real system. Pile 2 is modelled similarly to Pile 1, except that 32 Winkler springs are used to model the lesser embedded depth. The soil plug is taken the same as for Pile 1, as an added mass to a depth of 2 m below the original embedded length (i.e. a soil plug 5 m long from the pile tip). The impulse force is applied to a node in the model at a distance of 2 m below the pile head, in accordance to the real situation.

5.2. Example of applying the iterative updating method

An example of running the model is demonstrated in this section and the Pile 1 model with an initial starting soil stiffness estimate using the Biot approach (Eq. (2)) is shown. The results are presented in Fig. 7 for the first run of the model (with the random starting estimates for mass weighting), and the final converged values of F_a, since it is the acceleration FRF that is solely used in the procedure, see Section 3. To show that the method accurately calculates the operating parameters, F_v and F_d are also shown as calculated in the model overlain on the derived FRFs from the experimental data. Fig. 7(a) shows the experimental F_a and the first estimate of the numerical F_a. Fig. 7(b) and (c) show the same information for F_v and F_d respectively. Fig. 7(d) shows the experimental F_a and the converged numerical F_a. Fig. 7(e) and (f) show the same information for F_v and F_d. A plot of the initial estimate and final converged acceleration signal, used to develop the numerical F_a is shown in Fig. 8. Fig. 8(a) shows the predicted acceleration for the

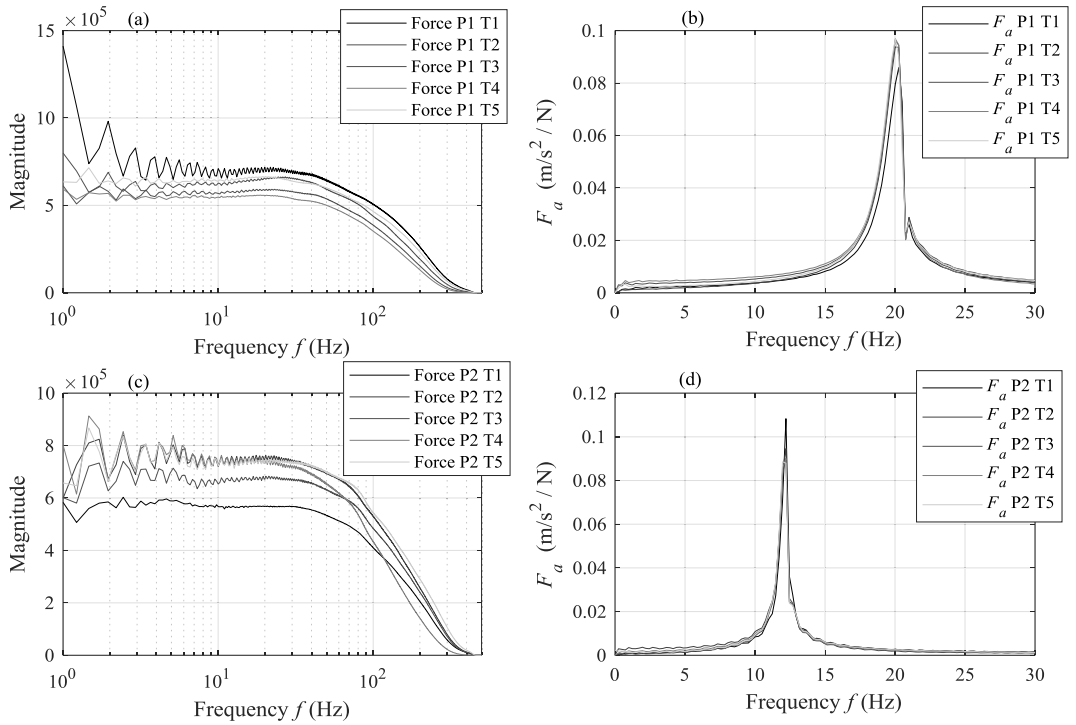

Fig. 4. Pile impact test data. (a) Frequency content of force time-history for five impact tests T1-T5 on Pile 1, (b) FRF from each impact test on Pile 1, (c) Frequency content of force time-history for five impact tests T1-T5 on Pile 2, (d) FRF from each impact test on Pile 2.

Table 1
Experimental data.

Test	Frequency (Hz)	Damping ratio (%) – curve fitting method
P1 T1	20.26	1.77
P1 T2	20.02	1.72
P1 T3	20.02	1.85
P1 T4	20.02	1.77
P1 T5	20.02	1.93
P2 T1	12.21	1.07
P2 T2	12.21	1.24
P2 T3	12.21	1.30
P2 T4	12.21	1.33
P2 T5	12.21	1.30

*P1 = Pile 1, P2 = Pile 2, T = Test No.

first iteration overlain on the experimental signal and corresponds to the FRFs shown in Fig. 7(a). Fig. 8(b) shows the final converged numerical acceleration overlain on the experimental signal and corresponds to the FRFs shown in Fig. 7(d). This figure demonstrates how the approach matches the real-measured response in the time-domain.

The method takes 21 iterations to converge (1 global loop of 15 iterations followed by resetting and 6 further iterations). The values of the parameters of interest (mass and stiffness weightings, ratios and tolerances) for all 21 iterations are reported in Table 2. The method stops when all three tolerances (mass, frequency and inferred stiffness, see Fig. 1) are less than 0.01 (1%). The method estimates that the Biot profile applied to the numerical model should be multiplied by 0.95 and soil mass equating to 6 times the pile mass should be distributed to the top quarter of the pile springs in order to match the experimental FRF.

5.3. Converged results for different starting stiffness profiles

In this section, the results of applying each of the five subgrade models (Eqs. (2)–(6)) as the initial starting estimate are trialled for Pile 1 and Pile 2. Each model is run one time, and the results of the converged mass and stiffness weightings for each stiffness profile and both piles are shown in Table 3. It is important to note that the converged stiffness weighting should be different for each model, as this is multiplied by the initial profile (Biot, Vesic, etc.) to obtain the converged soil stiffness profile. The mass weighting should be relatively consistent between runs, since this is multiplied by the constant that is the pile mass (for a given pile). In Table 3, it can be seen that for Pile 1, a relatively consistent estimate of the mass weighting is obtained from each model. The converged mass weighting for Pile 2 is a little more variable, though still reasonably consistent.

As mentioned above, it is expected the converged stiffness weightings be different for each model, as this is multiplied by the specified soil stiffness profile to obtain the converged stiffness profile. This is best demonstrated as in Fig. 9, which shows the starting and converged stiffness profiles with depth for each of the five subgrade reaction models for Pile 1. The stiffness is shown in terms of spring stiffness units (N/m). Fig. 9(a) shows the initial spring stiffness profiles (the markers show the individual springs) as derived from the site data in Fig. 2(b) using each subgrade model (Eqs. (2)–(6)). Fig. 9(b) shows the results of multiplying each of these profiles by the associated converged stiffness weighting for Pile 1 in Table 3. This plot demonstrates visually how the profiles converge toward one another to establish the *acting* soil stiffness for Pile 1.

5.4. Multiple runs for a given stiffness profile

The previous section presents the results of running each model once until convergence is achieved. However, since each run begins with effectively random starting estimates (between 0 and 30 for the mass weighting for the first run, and between 0.7 and 1.3 for the stiffness weighting for the second run), it is of interest to assess repeatability between multiple runs of a given model. Pile 1 with an initial stiffness profile defined by the Biot model (Eq. (2)) is run five times until converged mass and stiffness weightings are obtained. Fig. 10 shows the path of each weighting toward convergence for each run, Fig. 10(a) for the mass weightings and Fig. 10(b) for the stiffness weightings. Each run (R1-R5) takes a different number of iterations to

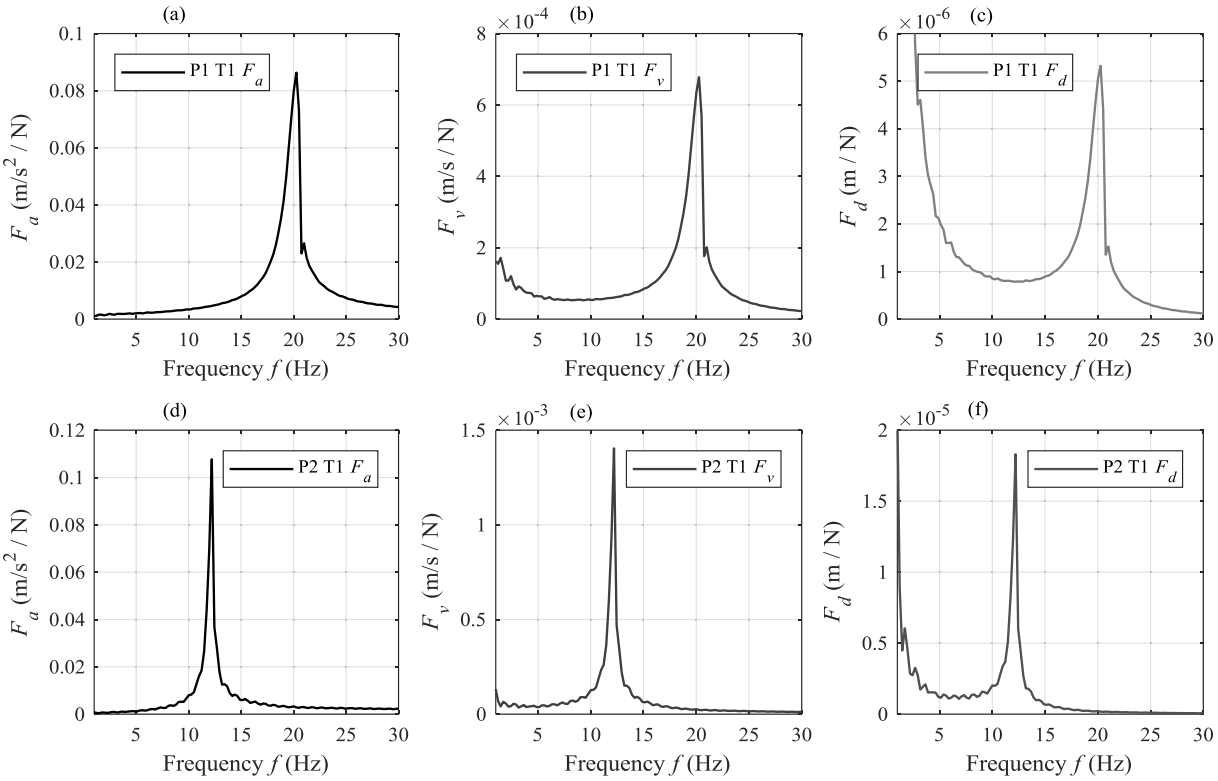

Fig. 5. Frequency Response Functions for the first impact test conducted on Pile 1 and 2. (a) Pile 1 F_a, (b) Pile 1 F_v, (c) Pile 1 F_d, (d) Pile 2 F_a, (e) Pile 2 F_v, (f) Pile 2 F_d.

converge. R1 takes 20 iteration to converge and ends with $w_m = 5.63$ and $w_k = 0.87$. R2 takes only 4 iterations to converge and ends with $w_m = 5.99$ and $w_k = 0.94$. R3 converges after 6 iterations with $w_m = 5.89$ and $w_k = 0.93$. R4 takes 5 iterations and converges with $w_m = 6.02$ and $w_k = 0.94$. Finally, R5 converges after 36 iterations with $w_m = 6.14$ and $w_k = 0.98$. Note also that the system resets if convergence is not achieved in 15 iterations, where all the parameters are reinitialised and the procedure starts over, see Fig. 1. The converged mass and stiffness weightings do vary a little between runs however in the context of obtaining stiffness information for geotechnical applications, they are reasonably consistent. Some of the reasons for the difference in the converged values is discussed in Section 5.7.

The results for the same analysis on Pile 2 is summarised in Table 4. The mass and stiffness weightings are reasonably consistent between runs for this pile with the Biot model.

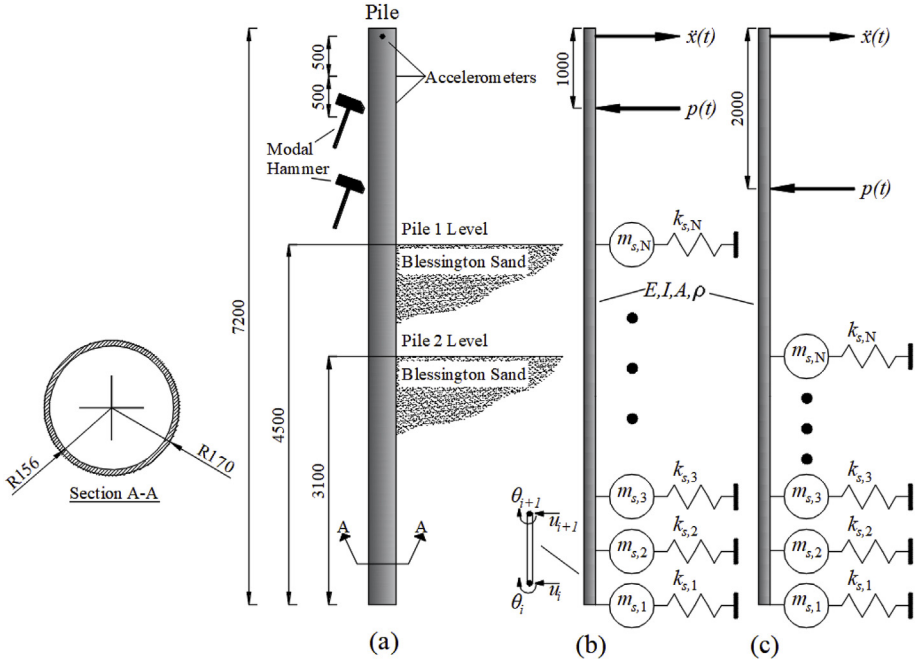

Fig. 6. Model schematic (dimensions in mm), (a) experimental pile geometry, (b) numerical schematic for Pile 1, (c) numerical schematic for Pile 2.

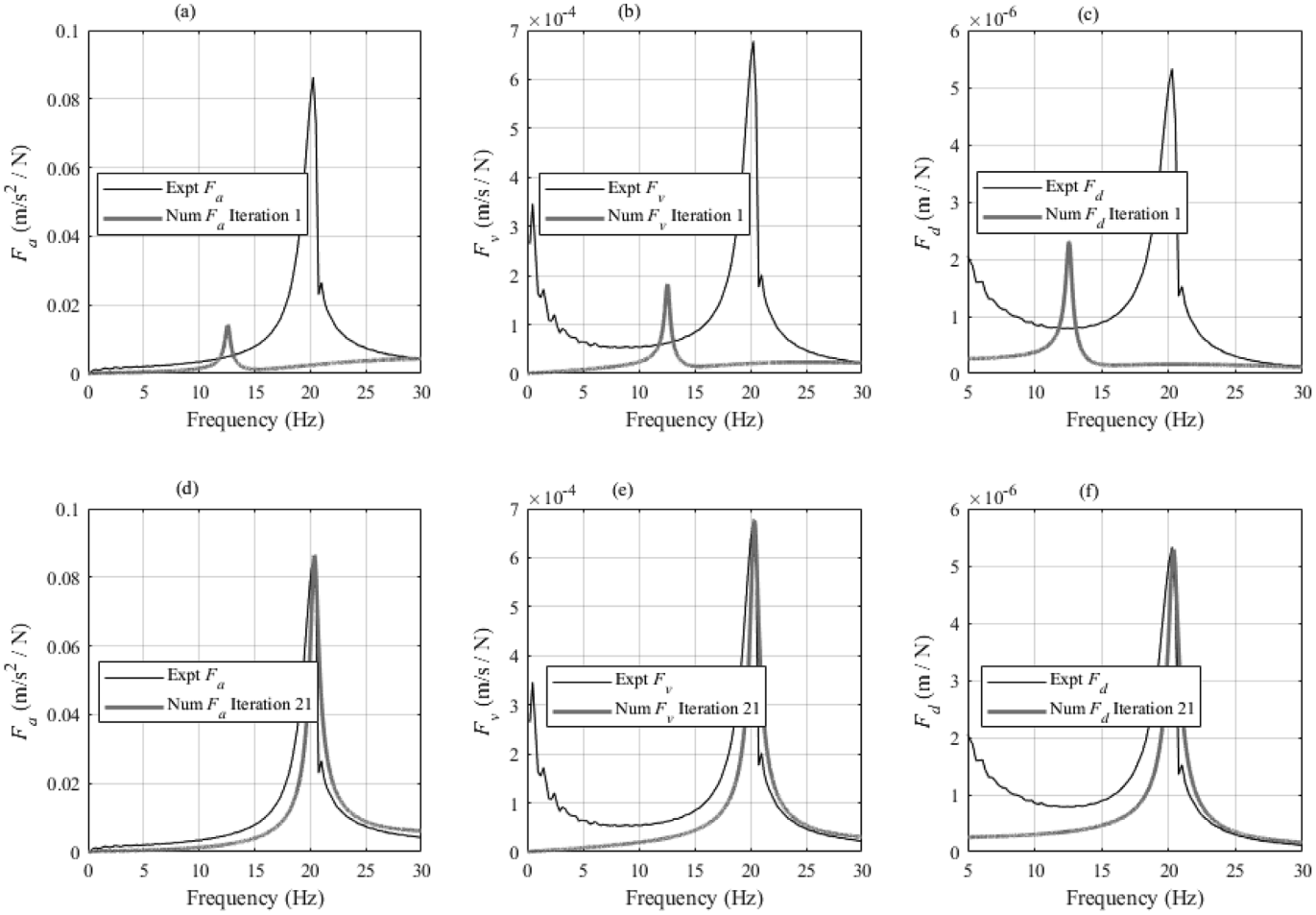

Fig. 7. Example of running the method for Biot starting profile – Pile 1. (a) F_a experimental and numerical iteration 1, (b) F_v experimental and numerical iteration 1, (c) F_d experimental and numerical iteration 1, (d) F_a experimental and converged numerical, (e) F_v experimental and converged numerical, (f) F_d experimental and converged numerical.

5.5. Consistency between different experimental impact tests

Until now, only one set of experimental data from each pile, namely F_a from 1 impact test (P1 T1 and P2 T1 Table 1) has been considered. In this section, the ability for the method to calculate consistent mobilised stiffness and mass weightings from a number of impact tests conducted on both Piles 1 and 2 is evaluated. The target FRFs for five impact tests are shown in Fig. 4. The method is run one time for each of the starting soil stiffness models (Eqs. (2)–(6)), for each of the five impact tests conducted on both piles (Table 1), resulting in a total of 50 runs. Table 5 shows the values of the converged stiffness and mass weightings from each run for Pile 1 and Table 6 shows the results for Pile 2.

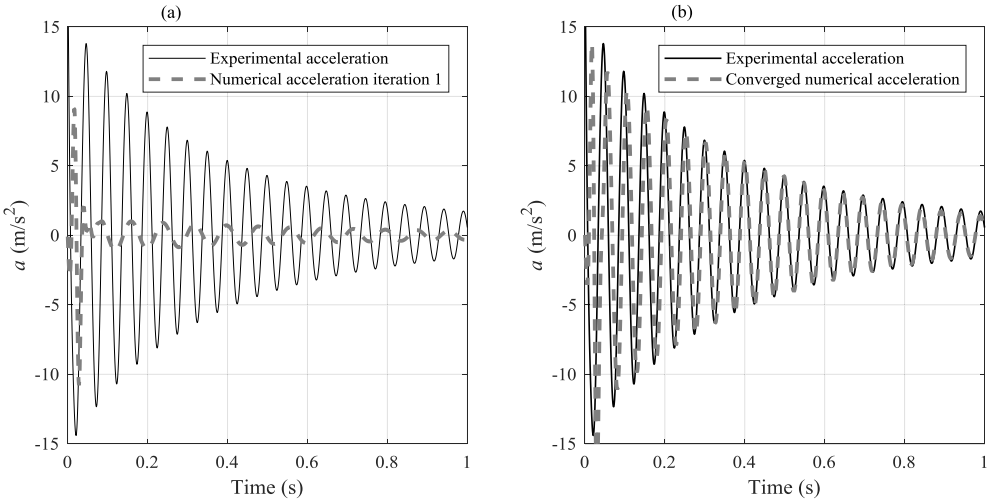

Fig. 8. Experimental and predicted accelerations – Pile 1. (a) Iteration 1 of the method, (b) Final iteration (21) of the method.

Table 2
Parameters during iterative process.

Global loop	Iteration	w_m	w_k	r_m	r_ω	r_k	Tol_m	Tol_ω	Tol_k
0	1	24.442	1.000	6.077	0.621	2.342	5.077	0.379	1.342
0	2	14.442	1.079	2.711	0.802	1.744	1.711	0.198	0.744
0	3	9.359	1.178	1.366	0.965	1.273	0.366	0.035	0.273
0	4	7.974	1.235	1.087	1.025	1.142	0.087	0.025	0.142
0	5	7.542	1.297	0.988	1.055	1.100	0.012	0.055	0.100
0	6	7.592	1.444	0.919	1.089	1.089	0.081	0.089	0.089
0	7	7.533	2.658	0.651	1.273	1.055	0.349	0.273	0.055
0	8	7.611	4.588	0.564	1.400	1.107	0.436	0.400	0.107
0	9	7.220	0.647	1.633	0.834	1.135	0.633	0.166	0.135
0	10	7.451	19.388	0.504	1.641	1.358	0.496	0.641	0.358
0	11	9.023	36.318	0.499	1.718	1.472	0.501	0.718	0.472
0	12	10.250	97.502	0.495	1.821	1.641	0.505	0.821	0.641
0	13	11.206	699.121	0.496	1.970	1.923	0.504	0.970	0.923
0	14	12.402	2236.178	0.498	2.029	2.049	0.502	1.029	1.049
0	15	13.486	10241.427	0.500	2.083	2.169	0.500	1.083	1.169
1	1	2.926	1.000	0.650	1.131	0.831	0.350	0.131	0.169
1	2	12.926	0.867	2.780	0.763	1.620	1.780	0.237	0.620
1	3	4.571	0.971	0.800	1.065	0.908	0.200	0.065	0.092
1	4	5.413	0.958	0.910	1.029	0.964	0.090	0.029	0.036
1	5	6.108	0.949	1.016	1.001	1.018	0.016	0.001	0.018
1	6	6.001	0.952	0.998	1.006	1.009	0.002	0.006	0.009

Table 3
Converged stiffness and mass weightings for one run of updating method for each subgrade reaction model – Pile 1 & 2.

Model	PILE 1		PILE 2	
	Converged w_k	Converged w_m	Converged w_k	Converged w_m
Biot	0.874	5.633	1.779	18.176
Vesic	1.266	5.838	2.399	17.790
Meyerhof & Baike	0.703	5.984	1.369	18.796
Klopple & Glock	0.377	5.858	0.847	20.915
Selvadurai	0.994	5.691	2.101	18.813

Observing Tables 5 and 6, the data from different impact tests lead to slightly different estimates of converged mass weightings in each case, for both piles. It is noteworthy that for a given impact test, the converged mass weightings for each of the soil stiffness models are relatively consistent for a given pile. There are two potential reasons for this, (i) the mass weighting is very sensitive to the quality of F_a and any variations in this strongly affect the converged mass weighting, or (ii) depending on the magnitude of the impact applied in each case, different amounts of mass may have been mobilised in the soil surrounding the pile. Converged stiffness weightings for a given soil profile also vary somewhat between impact tests. Further potential reasons for these differences are discussed in Section 5.7.

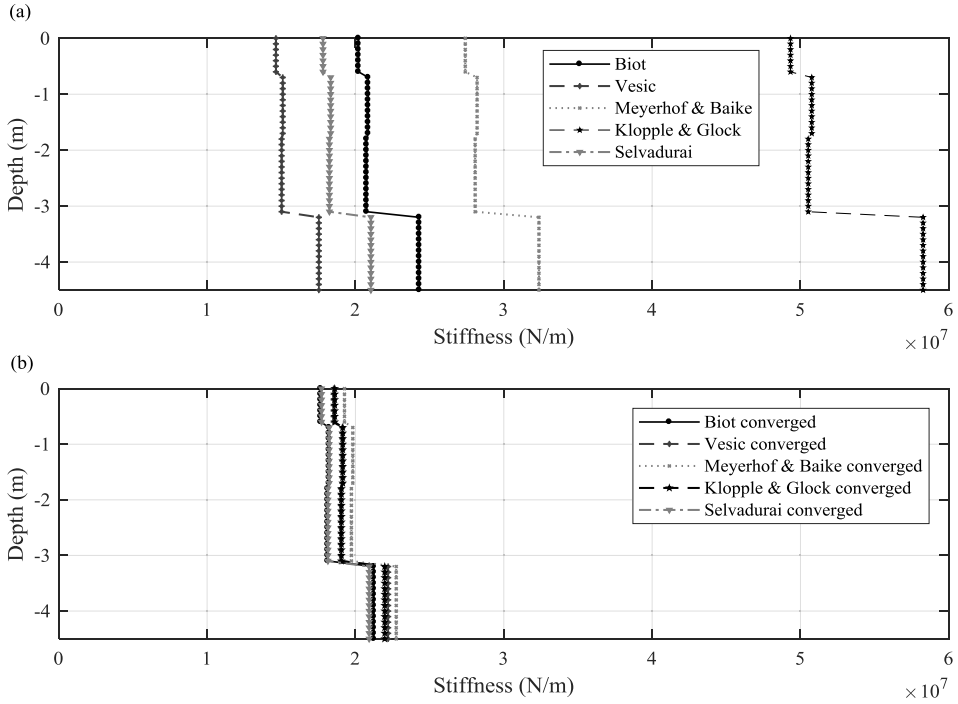

Fig. 9. Converged stiffness profiles after one run of each model - Pile 1. (a) Original stiffness profiles from each subgrade reaction formulation, (b) Converged weighted stiffness profile after one run of each model.

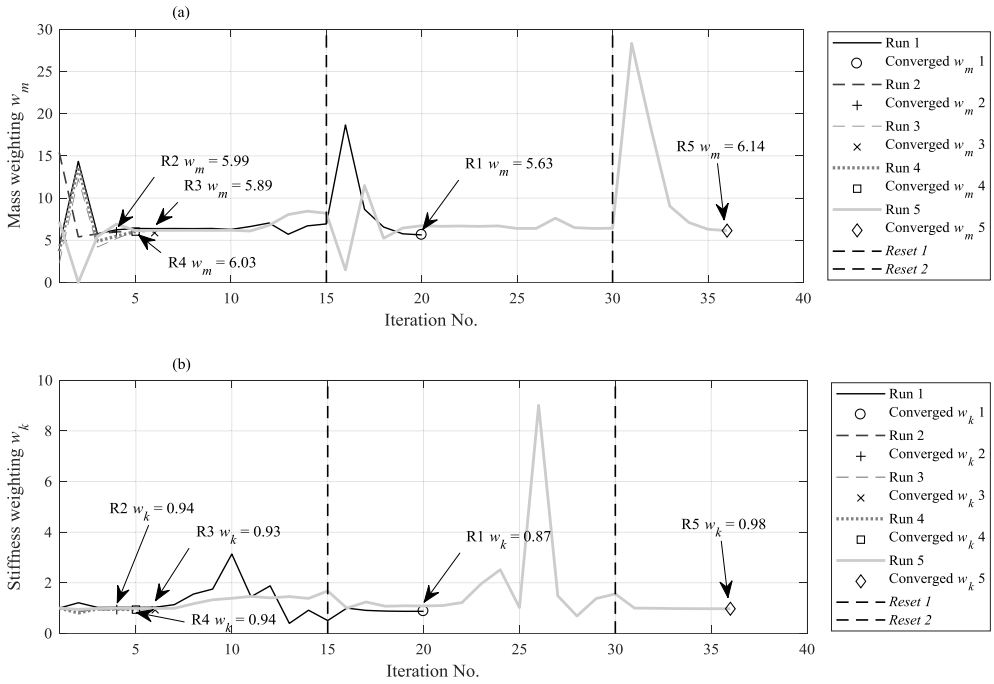

Fig. 10. Results of 5 runs of Biot model – Pile 1. (a) Convergence path for mass weighting for 5 runs of the model, (b) convergence path for stiffness weighting for 5 runs of the model.

Table 4
Results of 5 runs of Biot model – Pile 2.

Analysis run No.	w_m converged	w_k converged	Iterations
1	18.18	1.78	4
2	18.78	1.85	6
3	18.97	1.86	267
4	18.00	1.78	7
5	19.09	1.87	517

5.6. Influence of changing the active length over which masses are apportioned

All previous analyses consider the added soil masses apportioned to the top quarter of the springs in each model, as an approximate estimate for the mobilised mass of soil contributing to the first mode of vibration of each system. In reality, there will be some depth over which the soil mass will be effectively mobilised, due to the nature of the pile head bending when impacted. The active length, or effective depth of a pile, is the length beyond which further increases in pile length do not have any additional influence on pile head displacements, or rotations (or frequency) [52]. Quantifying the active length is an area of much uncertainty and previous studies have suggested several formulations for this parameter, which vary depending on the constraints applied to the pile head, the pile rigidity, and the nature of applied loading [53–58]. In this section, the influence of distributing masses over different lengths of a pile on the converged stiffness and mass weightings is studied. Active lengths equating to 25%, 50%, 75% and 100% of the embedded pile length are considered. Pile 1 impact test 1 (P1 T1, Table 1) is used as the test case and a Biot soil profile is adopted as the initial soil stiffness estimate. Each model is run five times for a given mass length distribution, and the results are presented in Table 7 as the average ± standard deviation of converged mass and stiffness weightings, for each mass distribution case.

Increasing the length over which masses are apportioned has limited influence on the converged stiffness weighting, with these values remaining sufficiently consistent for each case, considering the nominal errors present due to the natural variability in the algorithm convergence process. However, the converged mass weighting increases proportionally to the increase in mass distribution length, changing from $w_m = 5.83$ for masses distributed over 25% of the pile embedment to $w_m = 23.90$ for masses distributed along the entire embedded depth. In the procedure to add point masses to the pile, the mass weighting is multiplied by a fixed 'added mass', which is the pile mass, and this is then divided equally among the 'active spring nodes', namely the nodes with non-zero added masses. So, for the first case, a weighting of 5.83 is multiplied by the pile mass and divided among 12 springs (a quarter of the 46 springs), giving ≈ 0.5 times the pile mass added to each spring. For the last case, a weighting of 23.90 is multiplied by the pile mass and divided among all 46 springs, again giving ≈0.5 times the pile mass added to each spring. Therefore, when one normalises the converged weighting to the number of springs with non-zero added masses, the

Table 5
Pile 1 Analysis of five impact tests.

Impact Test No.	VESIC		SELVADURAI		BIOT		MEYERHOF		KLOPPLE	
	w_m	w_k	w_m	w_k	w_m	w_k	w_m	w_k	w_m	w_k
1	5.838	1.266	5.691	0.994	5.633	0.874	5.984	0.703	5.858	0.377
2	4.570	1.007	5.112	0.939	5.233	0.847	4.767	0.569	4.731	0.312
3	3.861	0.963	3.661	0.750	3.774	0.680	3.661	0.484	3.684	0.270
4	4.179	1.000	4.058	0.775	4.125	0.704	4.110	0.518	4.006	0.276
5	3.316	0.874	3.152	0.684	3.391	0.638	3.237	0.451	3.265	0.252

Table 6
Pile 2 Analysis of five impact tests.

Impact Test No.	VESIC		SELVADURAI		BIOT		MEYERHOF		KLOPPLE	
	w_m	w_k	w_m	w_k	w_m	w_k	w_m	w_k	w_m	w_k
1	17.790	2.399	18.813	2.101	18.176	1.779	18.796	1.369	20.915	0.847
2	16.763	2.375	16.203	1.881	18.413	1.829	17.606	1.323	17.862	0.738
3	17.959	2.486	17.918	2.045	17.771	1.790	17.991	1.334	17.649	0.710
4	15.771	2.366	15.625	1.905	15.371	1.670	14.932	1.199	16.107	0.708
5	15.220	2.030	15.376	1.686	14.249	1.379	15.757	1.104	15.633	0.622

Table 7
Influence of mass length distribution on converged weightings.

Masses distributed over length, L (L_p = pile length)	Average w_m ± Standard deviation	Average w_k ± Standard deviation
$L = 0.25L_p$	5.83 ± 0.27	0.92 ± 0.05
$L = 0.5L_p$	11.54 ± 0.39	0.92 ± 0.04
$L = 0.75L_p$	18.10 ± 0.70	0.97 ± 0.04
$L = L_p$	23.90 ± 0.44	0.97 ± 0.02

added point mass at each spring is approximately the same.

This finding highlights that no matter how many springs are specified to attach masses, the added point mass at each spring will be approximately the same. This result may seem counterintuitive as the global mass added increases with the number of active springs, and suggests that the approach is therefore very sensitive to the specified active length by the user. However, this result may be understood by observing the influence of added point masses on the F_a peak height for the first mode of the pile. Herein, the model for Pile 1 with a Biot stiffness profile subjected to an impact test is shown for the case where fixed point masses are added sequentially to the springs starting from ground level. The first run contains no added soil mass, the second run has one added mass, etc., until all the springs contain the same added point mass. With the increasing number of added masses, the FRF F_a peak height ($F_{a,max}$) decreases logarithmically, see Fig. 11. It is noteworthy that the peak heights, $F_{a,max}$ for the cases with masses added to 12 springs ($L/L_p = 0.25$) and masses added to 46 springs ($L/L_p = 1$) do not vary significantly, which explains why the result appears insensitive to the length over which masses are added. Note, to further investigate this influence would require observing higher modes of vibration, which would be influenced strongly by a given mass distribution. However, this is beyond the scope of the present study. It is recommended that potential users of the method specify an active length using the most applicable approach available.

5.7. Sources of error in the method

The iterative model updating approach presented in Ref. [23] was developed and validated using numerically simulated data of piles. Application of the approach to real experimental data has unearthed some issues. Variability and noise in experimental data inevitably affects the quality of results. One of the key issues may relate to the time-length of the signals available for the experimental analysis. The impact tests conducted on both piles contained 3 s of acceleration data. The impact of this is investigated in Figs. 12 and 13. Fig. 12(a) shows how the FRF F_a peak amplitude varies for different mass and stiffness weightings applied to the numerical model of Pile 1 with a Biot soil stiffness profile. The surface plot in Fig. 12(a) is generated using time signals of length $T = 200$s, the same as the analyses conducted throughout this paper. Also shown as a horizontal plane in grey is the peak amplitude of the experimental F_a as measured in the first impact test on Pile 1. An immediately obvious trait is that the numerical F_a peak amplitude is affected by changes in both mass and stiffness weighting, which deviates significantly from the theory of how single-degree-of-freedom (SDOF) models should behave, see Ref. [23]. The curve along which both the experimental and numerical planes intersect provides the solution combinations $\{w_m, w_k\}$, which lead to the same F_a peak amplitude in the numerical model as in the experimental data. It is important to note that the other criterion of matching the frequency is required in the iterative procedure, but not shown in these plots. This explains why the procedure always converges on broadly similar values for a given situation, and not a large range, as would be the case if the F_a peak alone were sought. Fig. 12(b) shows the same information as Fig. 12(a) but this time for the FRF F_d peak amplitude. The experimental data (horizontal grey plane) is the F_d peak amplitude derived from the experimental F_a using Eq. (9). Once again there is an intersection curve of $\{w_m, w_k\}$ combinations that enables the numerical model have the same F_d as the experiment. The influence of time on signal quality is investigated in Fig. 12(c) and (d), where an acceleration time series of length $T = 3$s is used for each run. The difference between the surface plots in (a) and (b) to those in (c) and (d) is best

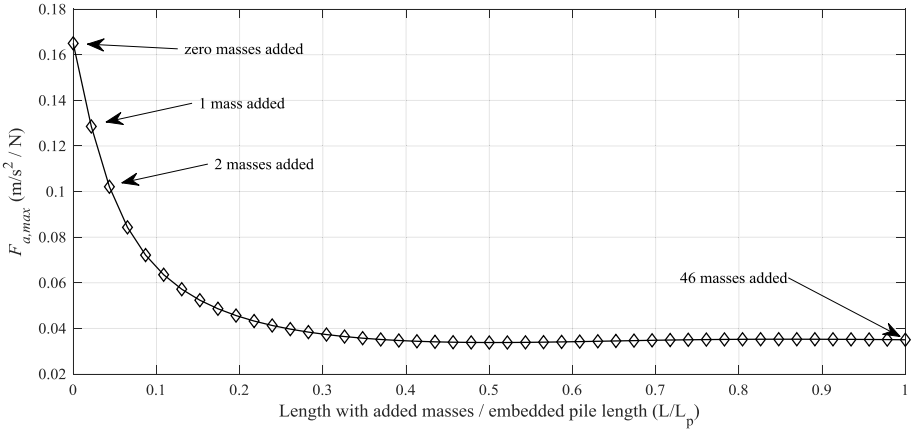

Fig. 11. Influence of increasing the number of added masses along the pile on the F_a peak value.

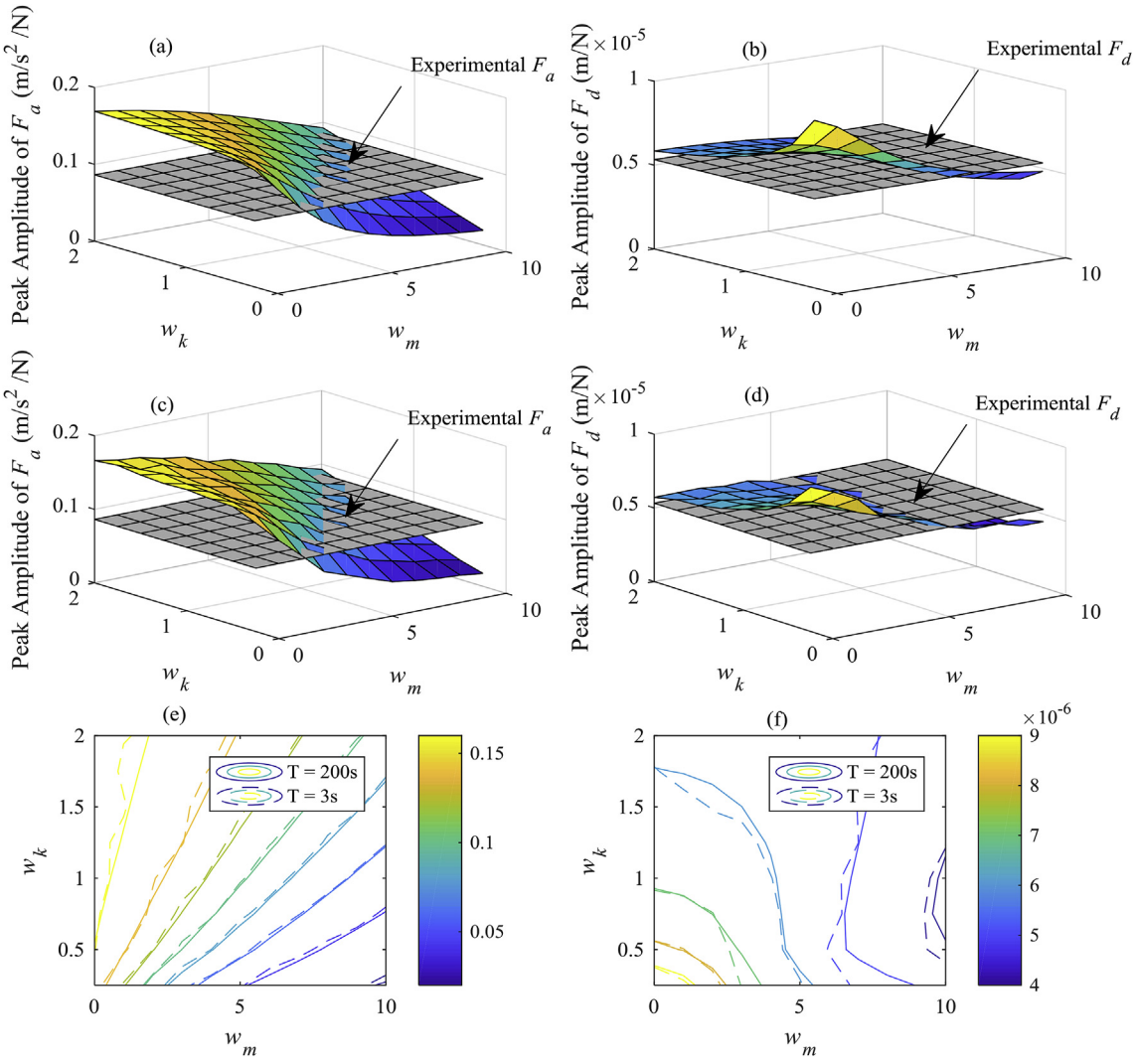

Fig. 12. Influence of signal length on FRF peak height for different mass and stiffness weightings for Pile 1 – Biot model. (a) Variation of peak amplitude of F_a with w_m and w_k compared to experimental F_a Impact Test 1 – T = 200s, (b) variation of peak amplitude of F_d with w_m and w_k compared to experimental F_d (derived) Impact Test 1 – T = 200s, (c) variation of peak amplitude of F_a with w_m and w_k compared to experimental F_a Impact Test 1 – T = 3s, (b) variation of peak amplitude of F_d with w_m and w_k compared to experimental F_d (derived) Impact Test 1 – T = 3s, (e) contour plot of peak amplitude of F_a with w_m and w_k for both T = 200s and T = 3s runs, (d) contour plot of peak amplitude of F_d with w_m and w_k for both T = 200s and T = 3s runs.

demonstrated in the contour plots shown in Fig. 12(e) and (f). The result of using a time series of length T = 200s for the analyses is shown by the smoothness of the solid contour lines in parts (e) and (f). Reducing the time series to T = 3s (in line with the experimental data) leads to a more jagged contour plot, denoted by the dashed lines in (e) and (f). This roughness in the peak F_a amplitude infers that for convergence to be achieved between the 'rough' experimental F_a and the 'smooth' numerical F_a some errors are introduced. For Pile 1 with a Biot stiffness profile, this is quite minor, however Fig. 13 shows the same information for Pile 2, which is significantly affected by signal length issues.

Fig. 13 shows the results for Pile 2 with a Biot soil stiffness profile. Fig. 13(a) shows a surface plot of the F_a peak amplitude and how it varies with mass and stiffness weightings. Fig. 13(b) shows this information for the F_d peak amplitude. Also shown as a horizontal grey plane is the experimental F_a peak amplitude in (a) and derived F_d peak amplitude in (b) from the first impact test on Pile 2. The smooth surface plots in (a) and (b) are derived from analysis of signals that are T = 200s long. Fig. 13(c) and (d) show the same information as (a) and (b) respectively, but are generated from time signals that are T = 3s long. For this case there is a substantial decrease in the smoothness of each plot, which highlights the potential errors that are introduced by the use of short time signals in the experimental data analysis. The results from the four surface plots in Fig. 13(a)-(d) are shown as contour plots in (e) and (f), where the solid contours are generated from T = 200s signals and the jagged contours from T = 3s. This highlights that use of the short experimental signals is a potential source of model error, which may be significant. This may account for some of the difference in calculated stiffness weightings between Pile 1 and 2. Note, all of the analyses in the previous sections used T = 200s for the numerical modelling while the experimental signals contained only 3 s of data.

While the short time-length of the processed signals may be the largest source of error, an additional source of error arises from the experimental impact testing. Each pile is an open-ended steel cylinder and, when subjected to impacts from a modal hammer, this induces an in-plane excitation in the pile annulus. This in-plane excitation manifests as a high-frequency pollution in the bending signal. Prior to transforming the time-signal to a FRF, the signal is low-pass filtered to remove the contribution of this noise [6,41]. This process will have some influence on the quality and nature of the FRF.

Further sources of error might arise due to the stepped nature of the

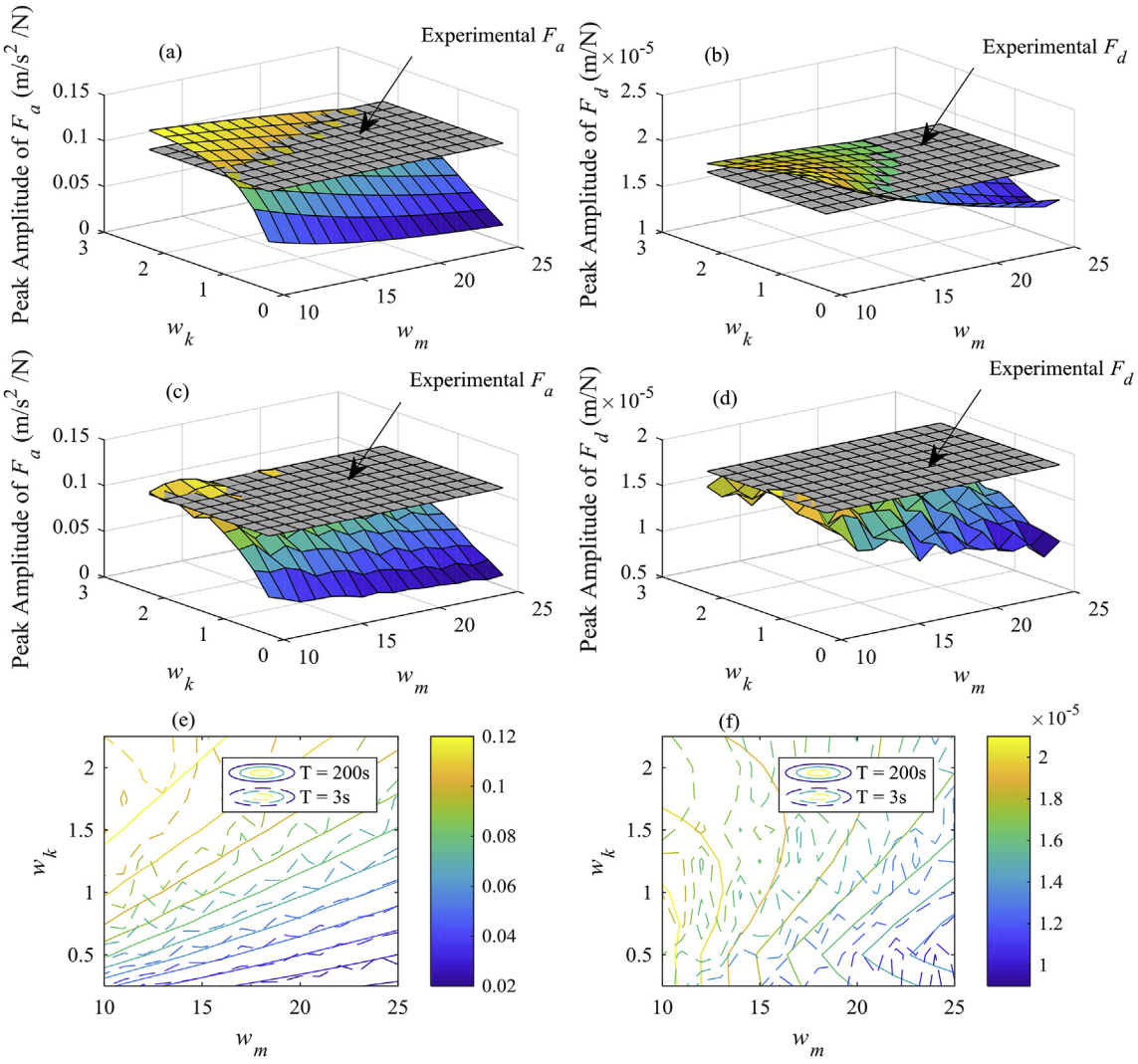

Fig. 13. Influence of signal length on FRF peak height for different mass and stiffness weightings for Pile 2 – Biot model. (a) Variation of peak amplitude of F_a with w_m and w_k compared to experimental F_a Impact Test 1 – $T = 200$s, (b) variation of peak amplitude of F_d with w_m and w_k compared to experimental F_d (derived) Impact Test 1 – $T = 200$s, (c) variation of peak amplitude of F_a with w_m and w_k compared to experimental F_a Impact Test 1 – $T = 3$s, (b) variation of peak amplitude of F_d with w_m and w_k compared to experimental F_d (derived) Impact Test 1 – $T = 3$s, (e) contour plot of peak amplitude of F_a with w_m and w_k for both $T = 200$s and $T = 3$s runs, (d) contour plot of peak amplitude of F_d with w_m and w_k for both $T = 200$s and $T = 3$s runs.

available soil stiffness (E) data from the multi-channel analysis of surface waves. Any errors here may be exacerbated in the procedure, which uses a single stiffness weighting for the entire profile depth. Moreover, since Pile 2 has less embedded depth than Pile 1, any errors in this profile will be exacerbated further. It should be noted that the same E profile is used for both piles, as this is in effect an average profile for the test site, so some errors can be expected as to the actual acting magnitudes at each depth. In terms of the *reference* numerical models developed, there is some question over the mass density of the internal plugged soil in each pile, which had to be estimated for the purposes of this paper. Additionally, the numerical method involves simplifying the pile to a 1D beam-Winkler system, which may deviate in behaviour from the real continuous pile system. Due to numerical constraints in iterative analyses of this nature, it is infeasible to use a full 3D model as it would be computationally too expensive.

6. Conclusion

In this paper, the application of a finite-element model updating approach to estimating the mobilised soil stiffness and mass in laterally impacted piles is studied. The reason behind the development of this method is due to the ongoing uncertainty surrounding the specification of soil-structure interaction stiffness in pile-soil interaction. Moreover, any contribution of soil mass is typically ignored. The method, which was previously derived and applied to simulated data, is demonstrated using experimental pile data in this paper.

Impact tests are performed on two piles with varying L/D ratios to derive frequency response functions, which are used as the target in an algorithm to estimate the mobilised soil stiffness and mass. Five subgrade reaction formulations are used to specify the initial starting stiffness. The analysis updates the soil stiffness and mass in a numerical model of the pile to converge on the experimental FRF. For the case where each of the five subgrade reaction models are used, the method converges on broadly similar added mass weightings and the converged stiffness profiles are relatively similar. This is better for Pile 1 than for Pile 2, which exhibits more variability (less embedded depth leads to more errors potentially). For a given impact test, the effect of running the model multiple times is studied to ascertain if significant variability exists between different runs. The results do vary a little, due to the random nature of the starting estimates for mass in the first iteration and stiffness in the second iteration, though the converged values are broadly similar for each trial. More variability is evident when different

impact tests are used as the target FRF for each case. In general, for a given impact test, the converged mass weighting for each subgrade reaction model is relatively similar for a given pile. However, the difference between the converged weightings for the different impact tests warrants some discussion. Experimental errors in the FRF peak height is most likely the reason for this variation, though there is potentially some influence from the amount of mobilised mass surrounding the pile as a result of the intensity of a given impact from the modal hammer. Additionally, the influence of the active depth over which masses are distributed is also investigated and it is shown for the conditions tested that masses distributed over a length beyond 20% of the embedment have limited further influence on the first mode of vibration. However, the effect on higher modes was not evaluated and would require further study. Finally, the sources of error due to time-length of signals is studied with a view to shedding some light on the importance of accurate experimental data. It is recommended that future studies use longer time signals for the experimental data than those available in the present study to mitigate against these signal-processing related issues. Short time signals lead to poorly spaced frequency vectors in the FRF, which may strongly influence the converged results.

Aside from some issues, the method was applied with relative success in this paper, and shows that a simple impact test may be useful to obtain better estimates of the mobilised soil-structure interaction stiffnesses and masses acting in the small-strain dynamic soil-pile behaviour. The research may be useful for the development of more accurate damage quantification models for SSI applications or in the growing offshore monopile fields.

Future work will investigate extension of the approach to use of multiple vibration modes to provide further insight into the behaviour and, to potentially enable depth-dependant weightings be obtained. The latter may be more useful for cases where large-strain deformations are experienced at pile heads relative to at-depth, thereby enabling calculation of the mobilised strain-dependant stiffness at the pile head. Furthermore, expansion of the approach to different types of foundation structures such as shallow pads or suction caissons should form part of future work. It should be noted that the approach in this paper uses an impact from a modal hammer to excite a structure; therefore there are some limitations of this approach. Large-diameter monopiles may not be sufficiently excited by impact from a modal hammer in order to obtain reliable FRFs. Moreover, highly damped systems suffer the same issues. Expansion of the approach to these types of systems may require investigation of different excitation sources to generate FRFs.

Acknowledgements

This research was enabled through funding obtained from the Royal Irish Academy Charlemont Scholarship Research Travel Awards 2016.

Appendix A. Supplementary data

Supplementary data to this article can be found online at https://doi.org/10.1016/j.soildyn.2019.04.027.

References

[1] Kampitsis AE, Sapountzakis EJ, Giannakos SK, Gerolymos N a. Seismic soil–pile–structure kinematic and inertial interaction—a new beam approach. Soil Dynam Earthq Eng 2013;55:211–24. https://doi.org/10.1016/j.soildyn.2013.09.023.
[2] Boulanger RW, Curras CJ, Kutter BL, Wilson DW, Abghari A. Seismic soil-pile-structure interaction experiments and analysis. J Geotech Geoenviron Eng 1999;125:750–9.
[3] Prendergast LJ, Reale C, Gavin K. Probabilistic examination of the change in eigenfrequencies of an offshore wind turbine under progressive scour incorporating soil spatial variability. Mar Struct 2018;57:87–104. https://doi.org/10.1016/j.marstruc.2017.09.009.
[4] Versteijlen WG, Metrikine AV, van Dalen KN. A method for identification of an effective Winkler foundation for large-diameter offshore wind turbine support structures based on in-situ measured small-strain soil response and 3D modelling. Eng Struct 2016;124:221–36. https://doi.org/10.1016/j.engstruct.2016.06.007.
[5] Allotey N, El Naggar MH. Generalized dynamic Winkler model for nonlinear soil–structure interaction analysis. Can Geotech J 2008;45:560–73. https://doi.org/10.1139/T07-106.
[6] Prendergast LJ, Gavin K. A comparison of initial stiffness formulations for small-strain soil – pile dynamic Winkler modelling. Soil Dynam Earthq Eng 2016;81:27–41. https://doi.org/10.1016/j.soildyn.2015.11.006.
[7] Zhu XQ, Law SS. Wavelet-based crack identification of bridge beam from operational deflection time history. Int J Solids Struct 2006;43:2299–317. https://doi.org/10.1016/j.ijsolstr.2005.07.024.
[8] Domaneschi M, Limongelli M, Martinelli L. Vibration based damage localization using MEMS on a suspension bridge model. Smart Struct 2013;12:679–94.
[9] OBrien E, Malekjafarian A. A mode shape-based damage detection approach using laser measurement from a vehicle crossing a simply supported bridge. Struct Contr Health Monit 2016;23(10):1273–86.
[10] Prendergast LJ, Hester D, Gavin K. Determining the presence of scour around bridge foundations using vehicle-induced vibrations. J Bridge Eng 2016;21. https://doi.org/10.1061/(ASCE)BE.1943-5592.0000931.
[11] Foti S, Sabia D. Influence of foundation scour on the dynamic response of an existing bridge. J Bridge Eng 2011;16:295–304. https://doi.org/10.1061/(ASCE)BE.1943-5592.0000146.
[12] Briaud JL, Hurlebaus S, Chang K, Yao C, Sharma H, Yu O, et al. Realtime monitoring of bridge scour using remote monitoring technology vol. 7. 2011. Austin, TX.
[13] Prendergast LJ, Hester D, Gavin K. Development of a vehicle-bridge-soil dynamic interaction model for scour damage modelling. Shock Vib 2016;2016. https://doi.org/10.1155/2016/7871089.
[14] Chen C-C, Wu W-H, Shih F, Wang S-W. Scour evaluation for foundation of a cable-stayed bridge based on ambient vibration measurements of superstructure. NDT E Int 2014;66:16–27. https://doi.org/10.1016/j.ndteint.2014.04.005.
[15] Imregun M, Visser WJ, Ewins. Finite element model updating using frequency response function data—I. Theory and initial investigation. Mech Syst Signal Process 1995;9:187–202. https://doi.org/10.1006/mssp.1995.0015.
[16] Nalitolela N, Penny JET, Friswell MI. Updating model parameters by adding an imagined stiffness to the structure. Mech Syst Signal Process 1993;7:161–72. https://doi.org/10.1006/mssp.1993.1005.
[17] Mottershead JE, Link M, Friswell MI. The sensitivity method in finite element model updating: a tutorial. Mech Syst Signal Process 2011;25:2275–96. https://doi.org/10.1016/j.ymssp.2010.10.012.
[18] Hwang HY, Kim C. Damage detection in structures using a few frequency response measurements. J Sound Vib 2004;270:1–14. https://doi.org/10.1016/S0022-460X(03)00190-1.
[19] Mottershead JE, Friswell MI. Model updating in structural dynamics: a survey. J Sound Vib 1993;167:347–75. https://doi.org/10.1006/jsvi.1993.1340.
[20] Esfandiari A, Bakhtiari-Nejad F, Rahai A, Sanayei M. Structural model updating using frequency response function and quasi-linear sensitivity equation. J Sound Vib 2009;326:557–73. https://doi.org/10.1016/j.jsv.2009.07.001.
[21] Lin RM, Zhu J. Model updating of damped structures using FRF data. Mech Syst Signal Process 2006;20:2200–18. https://doi.org/10.1016/j.ymssp.2006.05.008.
[22] Lin RM, Ewins DJ. Analytical model improvement using frequency response functions. Mech Syst Signal Process 1994;8:437–58. https://doi.org/10.1006/mssp.1994.1032.
[23] Wu WH, Prendergast LJ, Gavin K. An iterative method to infer distributed mass and stiffness profiles for use in reference dynamic beam-Winkler models of foundation piles from frequency response functions. J Sound Vib 2018;431:1–19. https://doi.org/10.1016/j.jsv.2018.05.049.
[24] Kwon YW, Bang H. The finite element method using MATLAB. Boca Raton, FL: CRC Press, Inc.; 2000.
[25] Winkler E. Theory of elasticity and strength. Dominicus Prague; 1867.
[26] Dutta SC, Roy R. A critical review on idealization and modeling for interaction among soil–foundation–structure system. Comput Struct 2002;80:1579–94. https://doi.org/10.1016/S0045-7949(02)00115-3.
[27] Clough RW, Penzien J. Dynamics of structures. 1993.
[28] Tedesco JW, McDougal WG, Allen Ross C. Structural dynamics: theory and applications. 1999.
[29] Dukkipati RV. Matlab for mechanical engineers. New Age Science; 2009.
[30] Biot MA. Bending of an infinite beam on an elastic foundation. J Appl Mech 1937;59:A1–7.
[31] Vesic AB. Bending of beams resting on isotropic elastic solid. J Soil Mech Found Eng 1961;87:35–53.
[32] Ashford SA, Juirnarongrit T. Evaluation of pile diameter effect on initial modulus of subgrade reaction. Geotech Geoenviron Eng 2003;129(3):234–42. https://doi.org/10.1061/(ASCE)1090-0241.
[33] Okeagu B, Abdel-Sayed G. Coefficients of soil reaction for buried flexible conduits. J Geotech Eng 1984;110(7):908–22. https://doi.org/10.1061/(ASCE)0733-9410.
[34] Sadrekarimi J, Akbarzad M. Comparative study of methods of determination of coefficient of subgrade reaction. Electron J Geotech Eng 2009;14.
[35] Elachachi SM, Breysse D, Houy L. Longitudinal variability of soils and structural response of sewer networks. Comput Geotech 2004;31:625–41. https://doi.org/10.1016/j.compgeo.2004.10.003.
[36] Donohue S, Long M, Gavin K, O'Connor P. Shear wave stiffness of Irish glacial till. Int. Conf. Site characterisation I. 2004. p. 459–66. Porto, Portugal.
[37] Prendergast LJ, Hester D, Gavin K, O'Sullivan JJ. An investigation of the changes in the natural frequency of a pile affected by scour. J Sound Vib 2013;332:6685–702https://doi.org/10.1016/j.jsv.2013.08.020i.
[38] Fugro. Guide for estimating soil type and characteristics using Cone penetration testing. 2011 Cone Penetration Tests http://www.fes.co.uk/downloads/CPT-general.pdf, Accessed date: 12 May 2014 accessed.

[39] Qi WG, Gao FP, Randolph MF, Lehane BM. Scour effects on *p–y* curves for shallowly embedded piles in sand. Geotechnique 2016;66:648–60. https://doi.org/10.1680/jgeot.15.P.157.
[40] Prendergast LJ, Gavin K, Doherty P. An investigation into the effect of scour on the natural frequency of an offshore wind turbine. Ocean Eng 2015;101:1–11. https://doi.org/10.1016/j.oceaneng.2015.04.017.
[41] Dezi F, Gara F, Roia D. Dynamic response of a near-shore pile to lateral impact load. Soil Dynam Earthq Eng 2012;40:34–47. https://doi.org/10.1016/j.soildyn.2012.04.002.
[42] Elsaid A, Seracino R. Rapid assessment of foundation scour using the dynamic features of bridge superstructure. Constr Build Mater 2014;50:42–9. https://doi.org/10.1016/j.conbuildmat.2013.08.079.
[43] Chopra AK. Dynamics of structures. A primer. Earthquake Engineering Research Institute; 1981.
[44] Gutenbrunner G, Savov K, Wenzel H. Sensitivity studies on damping estimation. Proc. Second int. Conf. Exp. Vib. Anal. Civ. Eng. Struct., Porto, Portugal. 2007.
[45] Doherty P, Kirwan L, Gavin K, Igoe D, Tyrrell S, Ward D, et al. Soil properties at the UCD geotechnical research site at Blessington. Proc. Bridg. Concr. Res. Irel. Conf., Dublin, Ireland. 2012. p. 499–504.
[46] Gavin KG, Lehane BM. Base load-displacement response of piles in sand. Can Geotech J 2007;44:1053–63.
[47] Gavin KGKG, O'Kelly BC, O'Kelly BC. Effect of friction fatigue on pile capacity in dense sand. J Geotech Geoenviron Eng 2007;133:63–71.
[48] Igoe D, Gavin K, O'Kelly B. The shaft capacity of pipe piles in sand. J Geotech Geoenviron Eng 2011;137:903–12.
[49] Gavin KG, Tolooiyan A. An Investigation of correlation factors linking footing resistance on sand with cone penetration results. Comput Geotech 2012;46:84–92.
[50] Gavin K, Adekunte A, O'Kelly B. A field investigation of vertical footing response on sand. Proc ICE, Geotech Eng 2009;162:257–67. https://doi.org/10.I680/geng.2009.I 62.5.257.
[51] Piezotronics PCB. Impulse hammer 086D50. Model 086D50 prod specif. 2018.
[52] Arany L, Bhattacharya S, Macdonald J, Hogan SJ. Design of monopiles for offshore wind turbines in 10 steps. Soil Dynam Earthq Eng 2017;92:126–52. https://doi.org/10.1016/j.soildyn.2016.09.024.
[53] Di Laora R, Rovithis E. Kinematic bending of fixed-head piles in nonhomogeneous soil. J Geotech Geoenviron Eng 2014;1–10. https://doi.org/10.1061/(ASCE)GT.1943-5606.0001270.
[54] Karatzia X, Mylonakis G. Discussion of "kinematic bending of fixed-head piles in nonhomogeneous soil" by raeffaele di laora and emmanouil rovithis. J Geotech Geoenviron Eng 2016;142:04014126https://doi.org/10.1061/(ASCE)GT.1943-5606.0001270.
[55] Goit CS, Saitoh M, Oikawa H, Kawakami H. Effects of soil nonlinearity on the active length of piles embedded in cohesionless soil: model studies. Acta Geotech 2014;9:455–67. https://doi.org/10.1007/s11440-013-0257-0.
[56] Velez A, Gazetas G, Krishnan R. Lateral dynamic response of constrained-head piles. J Geotech Eng 1983;109(8):1063–81. https://doi.org/10.1061/(ASCE)0733-9410.
[57] Gazetas G, Dobry R. Horizontal response of piles in layered soils. J Geotech Eng 1984;110(1):20–40. https://doi.org/10.1061/(ASCE)0733-9410.
[58] Randolph M. The response of flexible piles to lateral loading. Geotechnique 1981;31:247–59.